Electromagnetic induction noise in a towed electromagnetic streamer

GEOPHYSICS, VOL. 81, NO. 3 (MAY-JUNE 2016); P. E187–E199, 18 FIGS., 1 TABLE.
10.1190/GEO2014-0597.1

Electromagnetic induction noise in a towed electromagnetic streamer

Axel Tcheheumeni Djanni[1], Anton Ziolkowski[1], and David Wright[1]

ABSTRACT

We have examined the idea that a towed neutrally buoyant electromagnetic (EM) streamer suffers from noise induced according to Faraday's law of induction. A simple analysis of a horizontal streamer in a constant uniform magnetic field determined that there was no induction noise. We have developed an experiment to measure the induced noise in a prototype EM streamer suspended in the Edinburgh FloWave tank, and we subjected it to water flow along its length and to waves propagating in the same direction, at 45° and 90° to the streamer direction. The noise level was found to increase with increasing flow velocity. The motion of the prototype EM streamer in response to parallel constant current flow and wave motion was found to generate significant noise. The main finding is that wave motion was the major source of noise and was much larger than the noise of a static cable. The noise level can probably be reduced by towing the cable deeper and increasing the cable tension.

INTRODUCTION

Conventional marine controlled source electromagnetic (CSEM) data are acquired by deploying autonomous electric and magnetic field receiver nodes on the seafloor. A mobile horizontal electric dipole source (length 200–800 m) is towed approximately 50 m above the seabed (Constable and Srnka, 2007), and transmits a high-current (800–1500 A) low-frequency (0.01–1 Hz) EM field. The source magnitude is defined by the source dipole moment — the current multiplied by the source dipole length with units of amp meter (A-m). When the survey has been completed, the receivers are retrieved from the seafloor, and the recorded data are downloaded.

Conventional marine CSEM is time consuming to perform compared with 2D seismic surveying mainly because of the time it takes to deploy and recover the receiver nodes. In an effort to improve acquisition efficiency and reduce costs, a long flexible neutrally buoyant EM streamer cable has been developed to be towed simultaneously with an electric current dipole source at 4–5 knots (Anderson and Mattsson, 2010). The concept is illustrated in Figure 1. The EM streamer houses a series of electrode pairs distributed along its length, each connected by a telluric cable. The voltage between each pair of receiver electrodes is recorded. A towed system has also been developed by Constable et al. (2012) to provide information at near offsets (up to 1 km) during conventional CSEM surveying to enable better characterization of the near-surface resistivity, which is important in inversion of deeper data.

Although the increase in acquisition efficiency is obvious, the system is affected by noise from various sources. Therefore, its performance largely depends on noise levels in the acquired data. EM noise comprises all unwanted recorded voltages that degrade the desired signal transmitted through the earth. Connell and Key (2013) state that in conventional CSEM, the noise is directly related to (1) the environment and (2) the electronic logging system and the measurement electrodes. In the time domain, the noise $E_n(t)$ can be expressed as

$$E_n(t) = E_i(t) + \frac{V_r(t)}{l_r}, \qquad (\mathrm{V/m}), \qquad (1)$$

where $E_i(t)$ is the environmental electric noise field induced by sources such as the magnetotelluric (MT) signal, $V_r(t)$ is the combined voltage noise of the system electronics and the receiver electrodes, and l_r is the length of the electric receiver dipole. The MT signal is due to the time-variant incident magnetic field at the earth's surface. It originates in the ionosphere and magnetosphere and is spatially correlated over many kilometers (Gamble et al., 1979). The amplitude of the MT field increases rapidly with decreasing frequency that is less than 1 Hz (Simpson and Bahr, 2005) and

Manuscript received by the Editor 18 December 2014; revised manuscript received 22 November 2015; published online 06 April 2016.
[1]The University of Edinburgh, School of Geosciences, Grant Institute, King's Buildings, Edinburgh, UK. E-mail: tcheheumeni@gmail.com; anton.ziolkowski@ed.ac.uk; david.wright@geos.ed.ac.uk.

presents a problem for CSEM data acquired in shallow water where the MT signal is not attenuated by a thick conducting water layer.

When towing the receiver electrodes in the sea, there are other sources of noise which must be included. Equation 1 can be rewritten as

$$E_n(t) = E_i(t) + E_T(t) + \frac{V_r(t)}{l_r}, \qquad (\mathrm{V/m}), \qquad (2)$$

where $E_T(t)$ is the component of the electric field noise generated by the movement of the streamer in the earth's magnetic field. The sources of noise are summarized in Figure 2. For example, water currents and wave motion from surface waves can cause the streamer to deviate from a straight line. Another source of noise is cable tugging from the towing vessel. This is minimized as much as possible by a hydrodynamic depressor to decouple vessel motion from the streamer.

From equation 1 to equation 2, the noise levels increase substantially. Constable et al. (2012) find that data from a towed streamer in the frequency range 10–100 Hz are similar to data from stationary seafloor receivers, but the noise levels at 1 Hz are 1000 times larger that of a static node for data acquired with a 1 km long towed streamer. In this paper, noise is defined as what the receiver measures when there is no active source present.

Constable (2013) and Connell and Key (2013) suggest the length of the receiver dipole should be increased to reduce the noise generated by the logging system and measurement electrodes. The reason for this is clear from the second term on the right side of equation 1. This paper focuses on $E_T(t)$, which is unaffected by the dipole receiver length. It has been suggested that the EM induction voltage between a pair of receiver electrodes is the dominant source of noise in a towed streamer EM system (Burrows, 1974; Tenghamn et al., 2007; Engelmark et al., 2012). The induction voltage arises due to the motion of a conductor through the geomagnetic field, which induces an electric field of the form (Constable, 2013)

$$\mathbf{E} = \mathbf{v} \times \mathbf{B}, \qquad (3)$$

where $\mathbf{v}$ is the velocity of the conductor and $\mathbf{B}$ is the steady geomagnetic field. Two techniques using additional measurements have been proposed for reducing the induction noise (Ronaess and Lindqvist, 2010; Ziolkowski and Carson, 2014). However, neither of these patents estimate noise levels or the effectiveness of the technique.

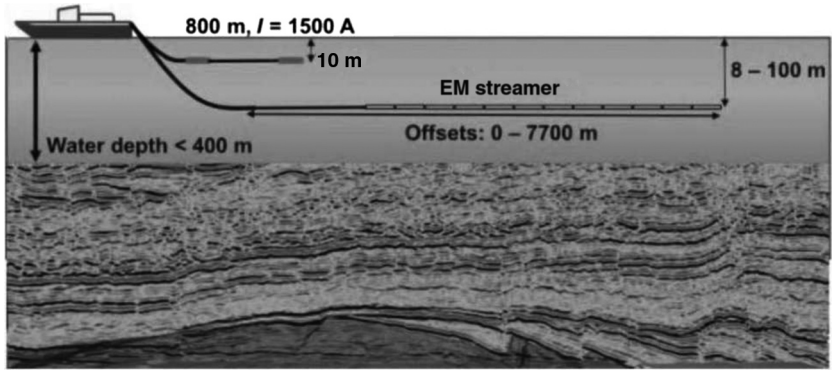

Figure 1. The towed streamer EM acquisition system. The source dipole is towed at a depth of 10 m and the streamer at a depth of 100 m or less. The receiver dipoles are 50–1100 m long with the length increasing with offset (Mattsson et al., 2012).

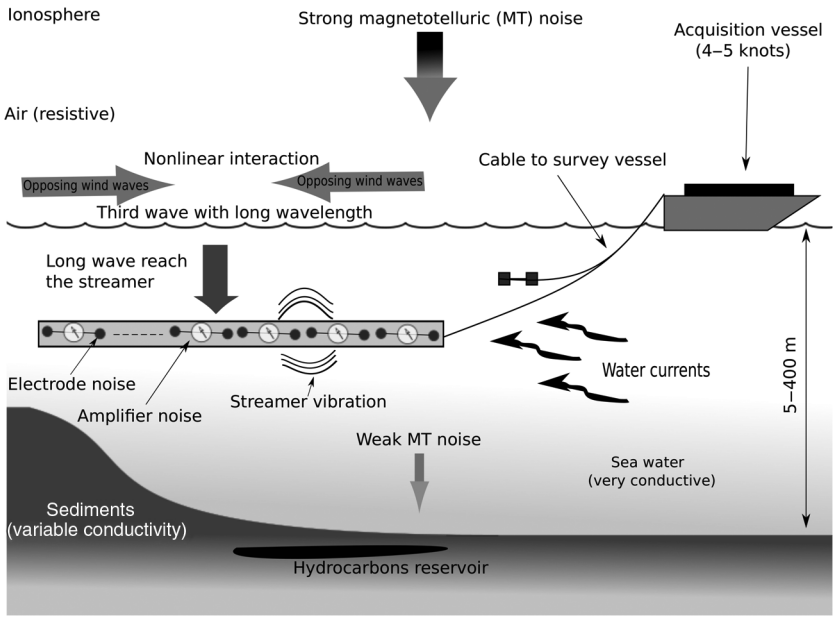

Figure 2. Sources of noise present in the towed EM system.

We seek to identify and quantify the contributions of noise caused by the flow of water over the receiver electrodes for different flow rates and the motion of the cable through the water in response to wave motion at different frequencies. We show that streamer motion is the major source of noise in the towed EM system.

We start with Faraday's law of induction and show its application in the case of a towed streamer EM system in a spatially invariant earth's magnetic field. Two cases are modeled to provide realistic examples. In the first case, we consider the streamer to be straight behind the vessel following the vessel's track. In the second case, the streamer is deviated from its track line because of crosscurrents present in the sea. Then, we present results of experiments carried out on a prototype EM streamer in the controlled environment of the FloWave tank with the purpose of understanding the nature and relative contributions of sources of noise originating from the flow around the streamer and the motion of the streamer in the earth's magnetic field.

THEORY OF INDUCED NOISE: FARADAY'S LAW OF INDUCTION

For our problem, two electrodes are connected by a cable in the presence of a spatially uniform magnetic field $\mathbf{B}(t)$, as shown in Figure 3. The earth's magnetic field does not vary spatially over the area S bounded by the loop of the cable, although it does vary with time. If the cable between the electrodes is not fully stretched, the straight line between the electrodes and the cable creates an electric loop C with an area S (Filloux, 1973).

When an electrode pair with contour C and area S moves with a velocity $\mathbf{v}$ in a time-varying magnetic field $\mathbf{B}(t)$, the general form of Faraday's law is expressed as (Cheng, 1989)

$$\mathcal{V} = -\frac{\partial}{\partial t}\int_S \mathbf{B}\cdot d\mathbf{S} + \int_C (\mathbf{v}\times\mathbf{B})\cdot d\mathbf{l}, \qquad \text{(V)}. \qquad (4)$$

In equation 4, all the terms are functions of time, and the term $\mathcal{V}$ is known as the electromotive force or induced voltage between the moving pair of electrodes. The first term on the right side is the induced voltage due to the time-varying magnetic field through the surface when the electrode pair is static. The second term is the induced voltage due to the motion of the electrode pair in the magnetic field. Because $\mathbf{B}(t)$ is a spatially uniform field, equation 4 can be written as

$$\begin{aligned}\mathcal{V} &= -\frac{\partial}{\partial t}(BS\cos(\widehat{\mathbf{n},\mathbf{B}})) + \int_{l_a}^{l_b}(\mathbf{v}\times\mathbf{B})\cdot d\mathbf{l}\\ &= -S\cos\alpha\left(\frac{\partial B}{\partial t}\right) - B\cos\alpha\left(\frac{\partial S}{\partial t}\right)\\ &\quad + BS\sin\alpha\left(\frac{\partial \alpha}{\partial t}\right) + \int_{l_a}^{l_b}(\mathbf{v}\times\mathbf{B})\cdot d\mathbf{l}, \qquad (5)\end{aligned}$$

where B is the magnitude of the geomagnetic field $\mathbf{B}$ within the area S, α is the angle between the geomagnetic field vector $\mathbf{B}$ and $\mathbf{n}$ the unit normal of the area S, l_a, and l_b are the electrode positions, and $\mathbf{v}$ is the velocity of the pair of electrodes relative to the earth.

From equation 5, it can be seen that the geomagnetic field induced noise voltage at each pair of electrodes can be generated in four ways: (1) a change in the magnetic field strength $(\partial B/\partial t)$, (2) variation in the surface area enclosed by the loop with time $(\partial S/\partial t)$ as illustrated in Figure 4a, (3) variation in the angle $(\partial\alpha/\partial t)$ between the magnetic field and the area vector with time, as shown in Figure 4b, and (4) acceleration of the moving conductor. During our experiment, the streamer was straight. Therefore, only (4) is applicable.

MOVING STREAMER IN A CONSTANT EARTH'S MAGNETIC FIELD

For a constant magnetic field $\mathbf{B}$ and enclosed area $\mathbf{S}$, the voltage induced between the receivers can be rewritten according to equation 4 as

$$\mathcal{V} = \int_C (\mathbf{v}\times\mathbf{B})\cdot d\mathbf{l} = \int_{l_a}^{l_b}(\mathbf{v}\times\mathbf{B})\cdot d\mathbf{l}, \qquad \text{(V)}, \qquad (6)$$

where $\mathbf{v}$ is the velocity of the streamer relative to the earth.

We consider $\mathbf{a_x}$, $\mathbf{a_y}$, and $\mathbf{a_z}$ as unit vectors in the x-, y-, and z-directions, respectively. Two cases are considered: First, when crosscurrents in the sea are insignificant, as shown in Figure 5a, and second, when the streamer is deviated from its track by crosscurrents as illustrated in Figure 5b.

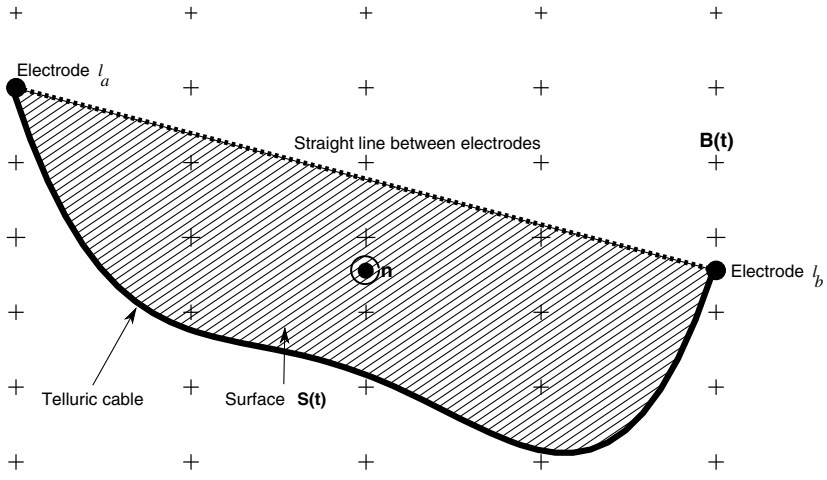

Figure 3. Electric loop created by the cable connected to the electrodes and the straight line between the electrodes (after Filloux, 1973). The magnetic field $\mathbf{B}$ is pointing downward (black crosses) and the normal to the surface $\mathbf{n}$ is pointing upward. The hatched area represents the surface S.

Case 1: No crosscurrent

The EM streamer is towed inline by a vessel at a nominal speed of 4–5 knots. The expressions for the differential length $d\mathbf{l}$, the geomagnetic field $\mathbf{B}$, and the velocity $\mathbf{v}$ are given by

$$d\mathbf{l} = \mathbf{a_x} dl_x, \tag{7}$$

$$\mathbf{B} = \mathbf{a_x} B_x + \mathbf{a_y} B_y + \mathbf{a_z} B_z, \tag{8}$$

$$\mathbf{v} = \mathbf{a_x} v_x + \mathbf{a_y} v_y + \mathbf{a_z} v_z. \tag{9}$$

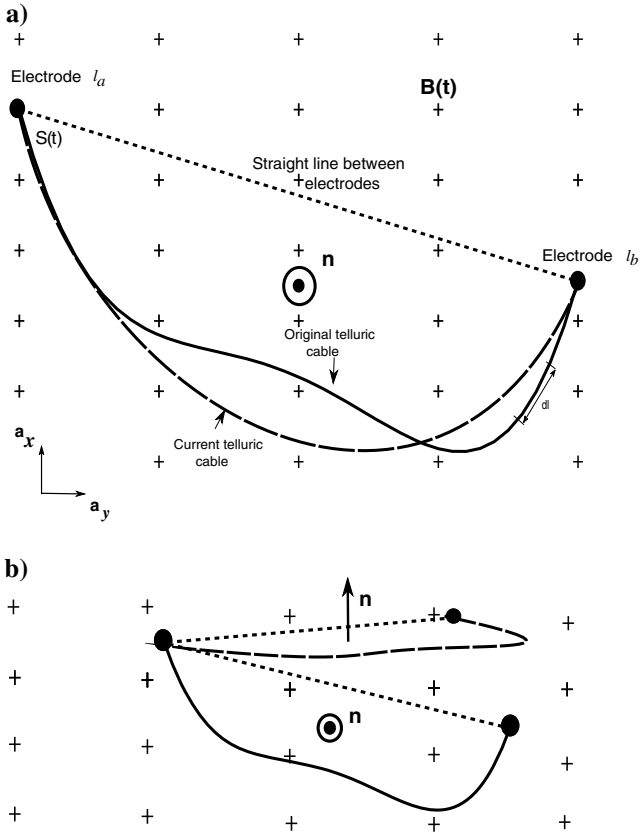

Figure 4. Illustration of two ways to generate an induced voltage according to Faraday's law of induction. (a) The surface area is changing over time. (b) The angle between **n** and **B** changes over time.

The streamer is towed in the inline direction; thus, $v_y = v_z = 0$. Therefore, equation 6 becomes

$$\mathcal{V} = \int_{l_a}^{l_b} (\mathbf{a_x} v_x \times \mathbf{a_z} B_z) \cdot \mathbf{a_x} dl_x = 0, \quad \text{(V)}. \tag{10}$$

That is, when the streamer is towed behind a vessel along the ship's track, the electrode pair cuts no magnetic flux. Therefore, no induced voltage is generated.

Case 2: With crosscurrent

A common problem in marine acquisition is currents that cause the streamer to deviate from its desired track line to a curved shape (Krail and Brysk, 1989) as illustrated in Figure 5b. The angle between the line from the vessel to the tail buoy and the line of the vessel's track is known as the feather angle (Krail and Brysk, 1989). The average feathering angle is generally less than 10° (Sheiman, 1990).

The velocity $\mathbf{v}$ and the geomagnetic field $\mathbf{B}$ do not change. However, the differential length $d\mathbf{l}$ becomes

$$\begin{aligned} d\mathbf{l} &= \mathbf{a_x} dl_x + \mathbf{a_y} dl_y \\ &= \mathbf{a_x} dl \cos\theta + \mathbf{a_y} dl \sin\theta, \end{aligned} \tag{11}$$

where $\theta \leq 10^{\circ}$ is the feather angle. Substituting equation 11 into equation 6 yields

$$\begin{aligned} \mathcal{V} &= \int_{l_a}^{l_b} (\mathbf{a_x} v_x \times \mathbf{a_z} B_z) \cdot (\mathbf{a_x} dl \cos\theta + \mathbf{a_y} dl \sin\theta), \\ &= -v_x B_z \sin\theta (l_b - l_a), \quad \text{(V)}, \\ \frac{\mathcal{V}}{L} &= -v_x B_z \sin\theta, \quad \text{(V/m)}. \end{aligned} \tag{12}$$

There is no time variation in equation 12; therefore, this generates only a DC shift in the induced voltage.

FLOWAVE TANK EXPERIMENT

This section provides a description of the experimental setup and equipment used during tests conducted at the FloWave tank in Edinburgh. The tank is 30 m in diameter, 3 m deep, filled with freshwater, and capable of generating flow rates of up to 1.6 m/s. Waves of different frequencies and amplitudes can be generated from any direction by 168 wave makers. These work to generate waves at one

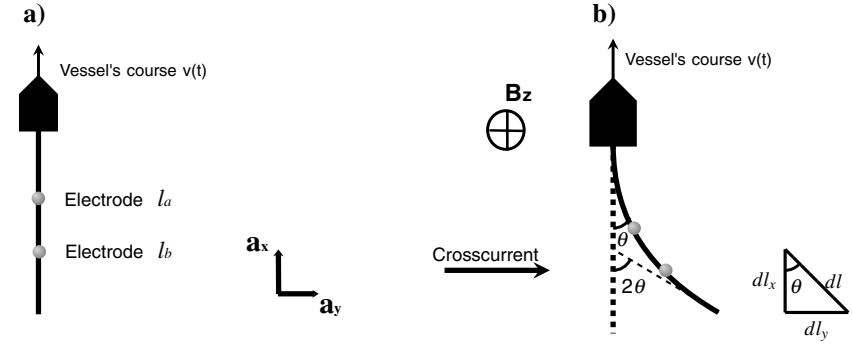

Figure 5. Cable profile dependent on sea conditions. (a) The streamer is in water without current. (b) The streamer profile is curved because of the crosscurrent.

side and to absorb waves at the opposite side to prevent any reflection of wave energy within the tank. Flow and wave motion can be generated simultaneously. The objective was to understand the behavior of an EM streamer section under the influence of flow and wave motion and to quantify their effects on the measured electric field.

Before making the measurements in the FloWave tank, a set of small-scale tests was conducted to ensure that the electrode performance was similar in saltwater and freshwater. In addition, the manufacturers confirmed that the electrodes were designed for use in both environments.

We built a 30 m long prototype EM streamer that was instrumented over the central 16 m section with 12 electric field channels (24 AgAgCl electrodes). The set-up is shown in Figure 6. In addition, three channels were fixed 1 m below the water surface. An anchor rope between the tank floor and the gantry was used to hold these electrodes in place. The telluric cable for these electrodes ran along the gantry and not through the water. Therefore, measurements made using these channels were not affected by any motionally induced noise that might affect receivers in the streamer section. Electrodes were connected to a 24 channel digital recording system with an 18 bit A/D converter sampling at 50 Hz. Five electrode wiring configurations were used during the test. Only results from the configuration shown in Figure 7a are presented here. There is an electrode at the center of the streamer, which is shared by all channels. Electrode separations range from 2 to 12 m; channels 13–15 are fixed electrode pairs with 6 m electrode spacing. Table 1 displays the relation between channel number and electrode spacing.

A prestretched Dyneema rope inside the streamer supports much of the tension within the streamer. The streamer is further anchored at each end by a three-point anchor between two points on the tank floor and the edge of the tank at ground level. This holds the streamer straight at a depth of 1 m. Figure 7b shows the streamer being deployed in the tank.

Motion of the EM streamer

The central 4 m section of the streamer was further instrumented with 21 reflective markers to monitor cable motion using Qualisys underwater infrared motion-capture cameras. The locations of these markers are shown in Figure 8a. The cameras record the x, y, and z positions of the reflectors to a precision of ± 2 mm at a distance of 10 m. The positions of the markers are defined by a right-handed Cartesian coordinate system as shown in Figure 8b. The x-direction is aligned with the streamer, whereas the z-direction is in the vertical upward direction.

Increased flow rates and wave motion

Two tests were carried out to investigate the effect on noise levels of increasing water flow rate and wave motion at different frequencies and amplitudes around the streamer.

1) Test 1: The effect of flow. Water flow was generated parallel to the streamer. Data were acquired for flow rates of 0, 0.5, 1, and 1.5 m/s.
2) Test 2: The effect of wave motion. Data were acquired with a constant flow rate of 0.5 m/s parallel to the streamer and a 0.1 m wave amplitude. Wave frequencies of 0.29 and 0.45 Hz were generated (1) in the flow direction, (2) opposite to the flow direction, (3) 45° to the flow direction, and (4) 90° to the flow direction.

The motion of the streamer was recorded simultaneously with the electric field to investigate the relation between the electric field noise and cable motion.

EXPERIMENTAL RESULTS

Streamer displacement

The mean displacement of each component was first subtracted so that the signal fluctuates around zero. Figure 9 displays the displacement markers for flow rates of 0.5 (Figure 9a), 1 (Figure 9b), and 1.5 m/s (Figure 9c). Figure 10 shows the displacement markers for a constant flow (0.5 m/s) parallel to the streamer and a 0.1 m wave propagating in the direction of the flow. Figure 11 shows the same result for a wave propagating at 90° to the direction of the flow (x-direction). Results are shown for wave frequencies of 0.29 (Figure 11a) and 0.45 Hz (Figure 11b).

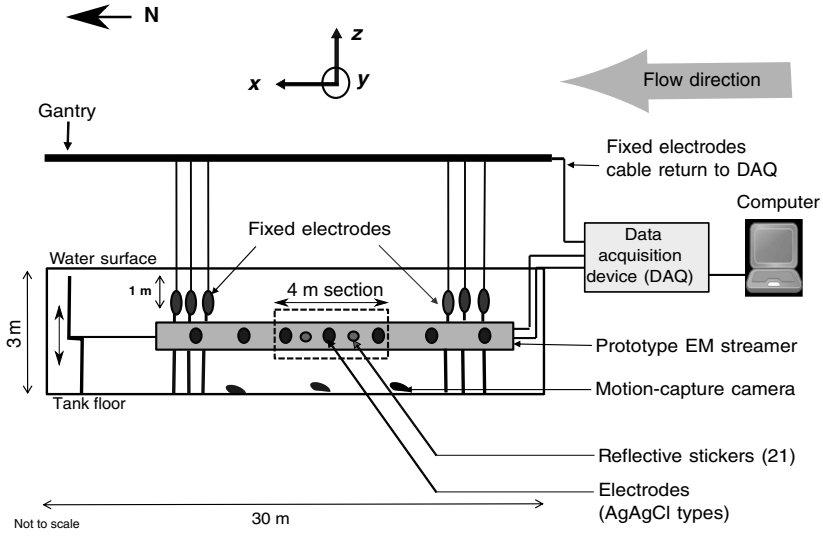

Figure 6. Configuration of the EM streamer in the FloWave tank showing the fixed electrodes and reflector sticker for the motion-capture cameras. The dashed rectangular section represents the 4 m section, where the motion of streamer was recorded. The flow is parallel to the streamer.

As flow rates increased from 0.5 to 1.5 m/s, displacements in the x- (Figure 9, bottom) and z-directions (Figure 9, top) were not affected by water passing through the streamer. Meanwhile, the displacement in the y-direction (Figure 9, middle) showed a small increase as flow increased from 0.5 ($\pm$0.01 m) to 1.5 m/s ($\pm$0.02 m). However, the displacement remained constant from 1 to 1.5 m/s.

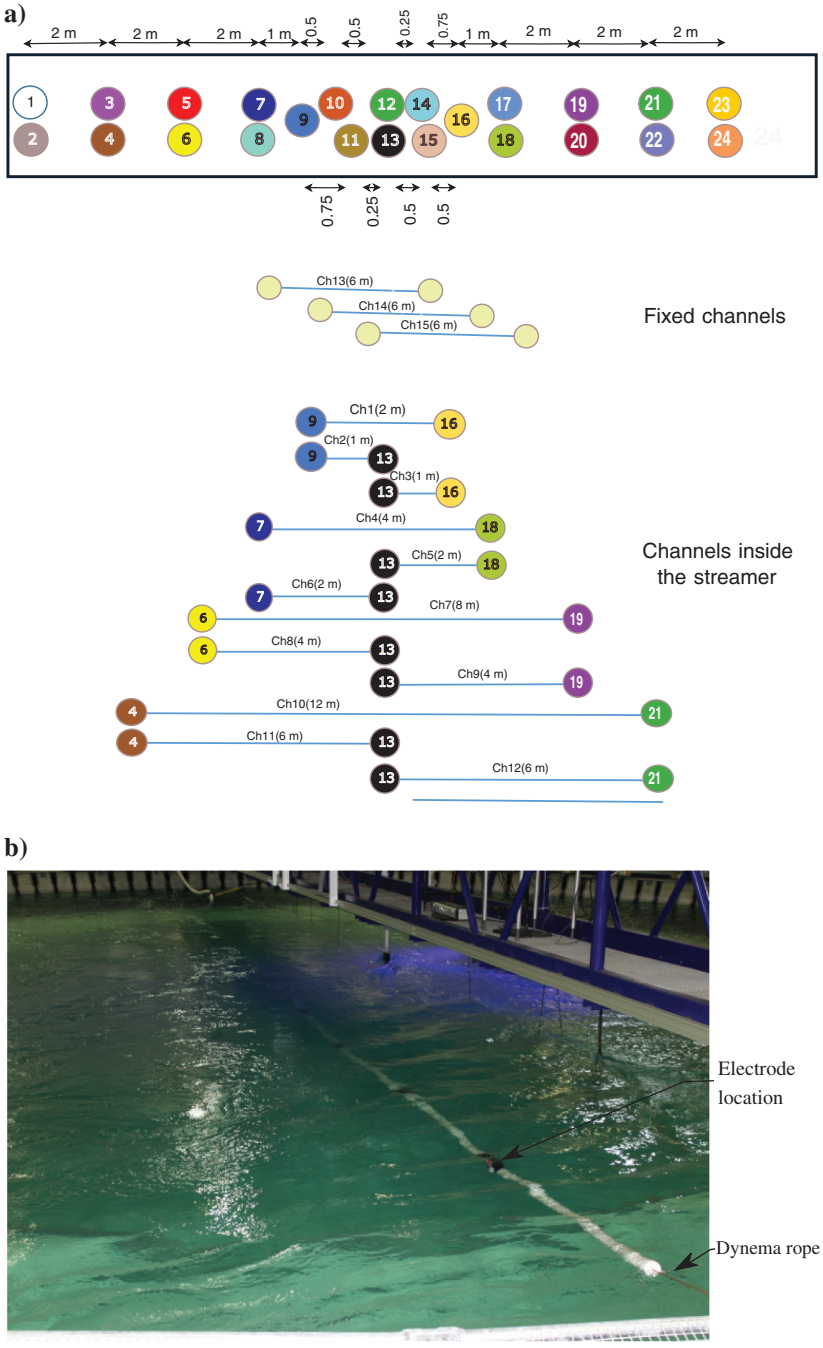

Figure 7. (a) Layout of the wiring configuration. Channels 13–15 are fixed channels (not to scale). (b) Photo of the prototype streamer (white cable) being deployed in the FloWave tank. The Dyneema rope and the location of electrodes are indicated.

Table 1. Relationship between channel number and electrode spacing.

Channel	Ch 1	Ch 2	Ch 3	Ch 4	Ch 5	Ch 6	Ch 7	Ch 8	Ch 9	Ch 10	Ch 11	Ch 12	Ch 13	Ch 14	Ch 15
Electrode spacing (m)	2	1	1	4	2	2	8	4	4	12	6	6	6	6	6

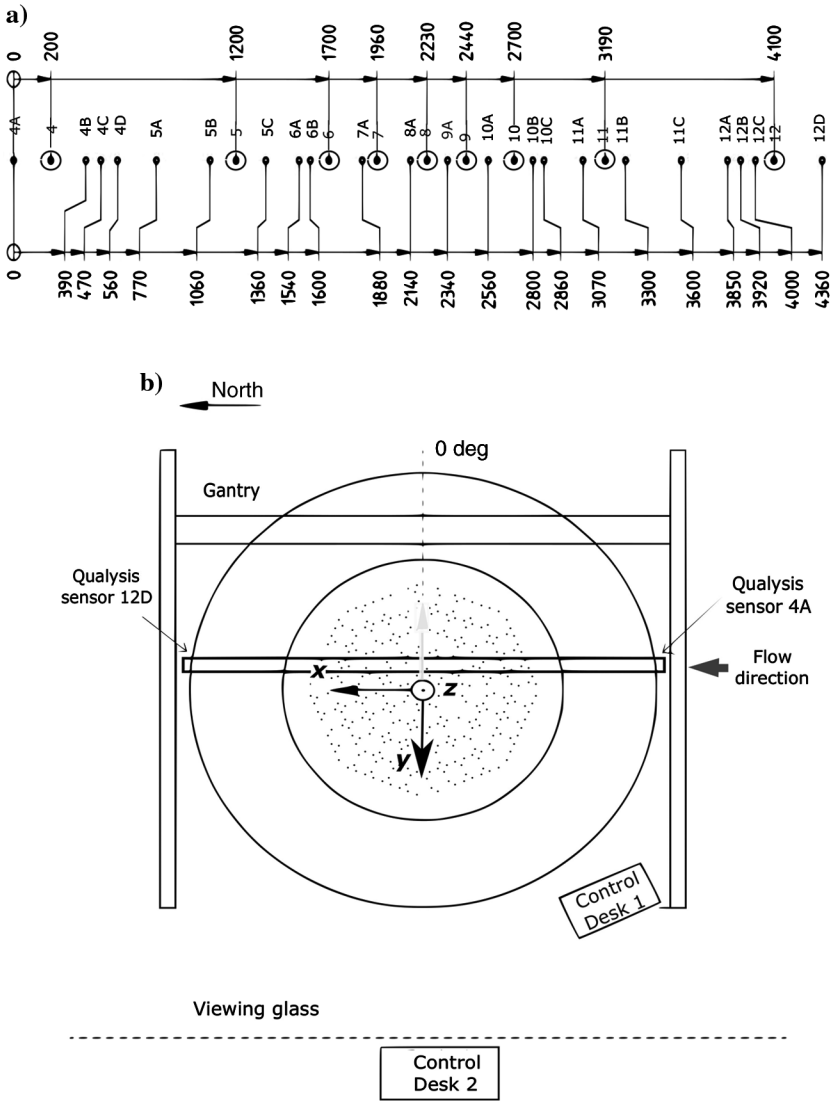

Figure 8. (a) Sketch of the 4 m section of the streamer. The round black spots denote the motion sensors, and the circle black spots represent electrodes. (b) Layout and coordinate system for the motion detection cameras. The streamer is oriented north–south. The arrow on the right hand side indicates the origin of flow.

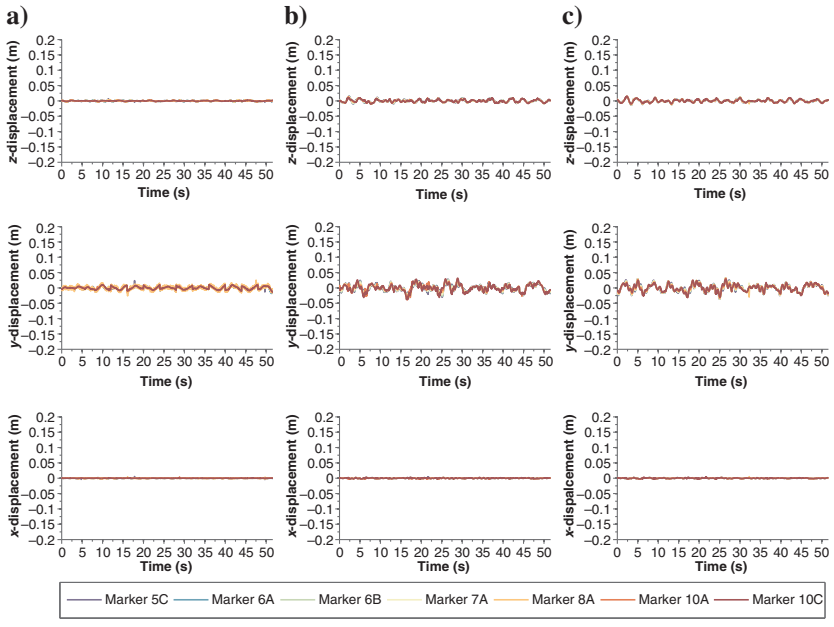

Figure 9. Time series in the z-, y-, and x-direction for seven markers in response to flow rates of (a) 0.5, (b) 1, and (c) 1.5 m/s, respectively. The data were recorded in the absence of wave motion.

Regardless of wave frequency, the largest displacement is measured along the *y*-direction when the wave propagates in the *y*-direction (Figure 11). This displacement is an order of magnitude larger than when the wave propagates in the *x*-direction (Figure 10). Displacement in the *z*-direction is the same for different wave frequencies.

The amplitude spectra of the data in Figures 10 and 11 are shown in Figures 12 and 13. For an input wave of 0.29 Hz (Figures 12b and 13b), there is a peak in the amplitude spectrum at the wave frequency and the first and second harmonics of 0.58 and 0.87 Hz, respectively. This is due to the streamer setting up a standing wave at these frequencies because of being anchored at each end.

These results indicate that the streamer is more sensitive to the wave motion than to an increase in flow parallel to the streamer with particular sensitivity to wave motion perpendicular to the streamer.

3D motion of the streamer

It is difficult to visualize streamer motion from displacement of a single component. A more intuitive way to display the displacement is to plot displacement of two components as a function of time. Figure 14a and 14b shows displacement of a single marker in the *y*-*z* and *x*-*z* plane for a wave propagating parallel to the streamer. Figure 14c and 14d shows displacement of the same marker in the *y*-*z* and *x*-*z* plane for a wave propagating perpendicular to the streamer. Displacement in the *x*-direction is almost zero as the streamer is under tension. It can be seen that when the wave propagates parallel to the streamer axis, the horizontal and vertical displacements are similar in amplitude and oscillate at the wave frequency. When wave motion is perpendicular to the streamer, the *y*-displacement increases by a factor of 10, whereas the *z*-displacement increases only slightly.

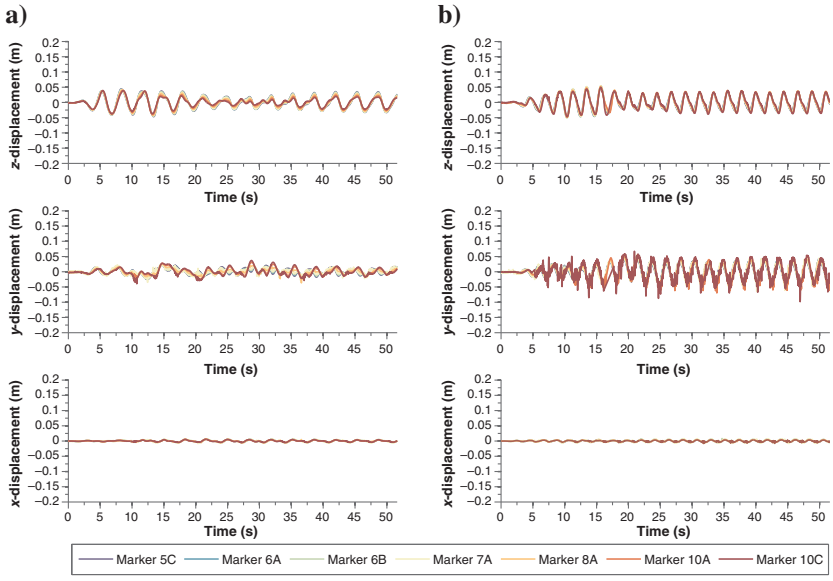

Figure 10. Time series in the *z*-, *y*-, and *x*-direction for seven markers in response to wave motion of amplitude 0.1 m traveling along the streamer. Panels (a and b) show wave frequencies 0.29 and 0.45 Hz, respectively.

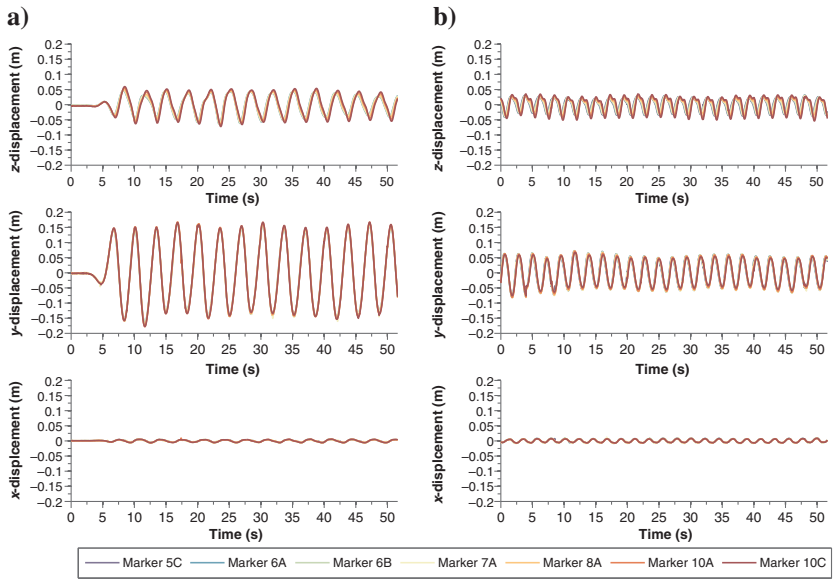

Figure 11. Time series in the *z*-, *y*-, and *x*-direction for seven markers in response to wave motion perpendicular to the streamer. Panels (a and b) show wave frequencies 0.29 and 0.45 Hz, respectively.

Flow rate analysis

The distribution of noise along a streamer can be obtained by averaging the root-mean-square (rms) values from several statistically independent records (e.g., Elboth et al., 2009).

To compute the mean rms, the following steps were implemented:

1) A low-pass filter was applied to the data to remove signals higher than 10 Hz.
2) The 70 s noise records were divided into two equal 35 s windows.
3) DC was removed in each window.
4) Rms was calculated in each window.
5) Standard deviation and standard error were computed to give a measure of the rms variability.

Analysis of the results indicated that channels 2, 3, 7, and 10 may be faulty. We, therefore, excluded them from our analysis. Data were acquired for flow rates of 0, 0.5, 1, and 1.5 m/s. The same analysis was applied to data recorded with a 0.29 Hz wave propagating in the streamer direction. The results are shown in Figures 15 and 16.

From Figures 15 and 16, it can be seen that the rms electric field noise levels recorded without flow and wave motion (blue bar on the graphs) vary from channel to channel. This noise corresponds to $E_n(t)$ in equation 1. Because the environmental electric noise field due to the MT signal ($E_i(t)$) is the same for all channels, it

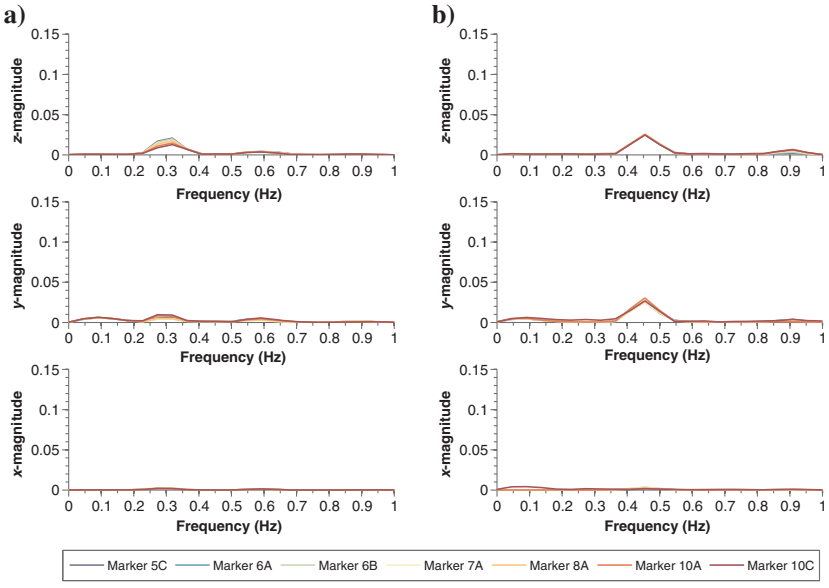

Figure 12. Amplitude spectrum of the z-, y-, and x-displacement data shown in Figure 10. Panels (a and b) show wave frequencies 0.29 and 0.45 Hz, respectively. Note the large frequency peak at the wave input frequency (0.29 and 0.45 Hz, respectively).

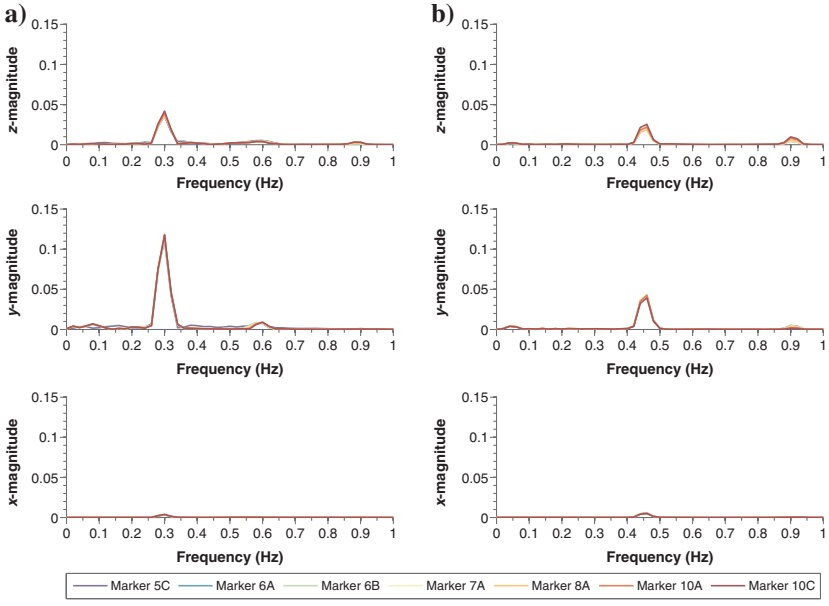

Figure 13. Amplitude spectrum of the z-, y-, and x-displacement data shown in Figure 11. Panels (a and b) show wave frequencies 0.29 and 0.45 Hz, respectively. Note the large frequency peak at the wave input frequency (0.29 and 0.45 Hz, respectively).

is reasonable to assume that any discrepancy between channels is due to electrode noise at each channel.

From Figure 15, it can be seen that the rms noise increased by approximately 40% as the flow increased from 0 to 1.5 m/s. However, most of this increase occurs between no flow and flow of 0.5 m/s. The increase in noise is mainly due to increased water motion around the streamer. Extrapolating these results to a flow rate of 2.5 m/s at which towed streamer data are acquired suggests an increase in the noise level (due to E_T in equation 2) of 45% above the static noise level (E_n in equation 1). The effect of a constant flow of 0.5 m/s and wave motion is shown by the green bar in Figure 15. It is clear that wave-related noise is more than twice that of flow-related noise. As the receiver length increases, the relative contribution of flow noise decreases because it is independent of receiver length.

The effects of waves traveling in different directions relative to the streamer are shown in Figure 16. The rms noise level, due to E_T

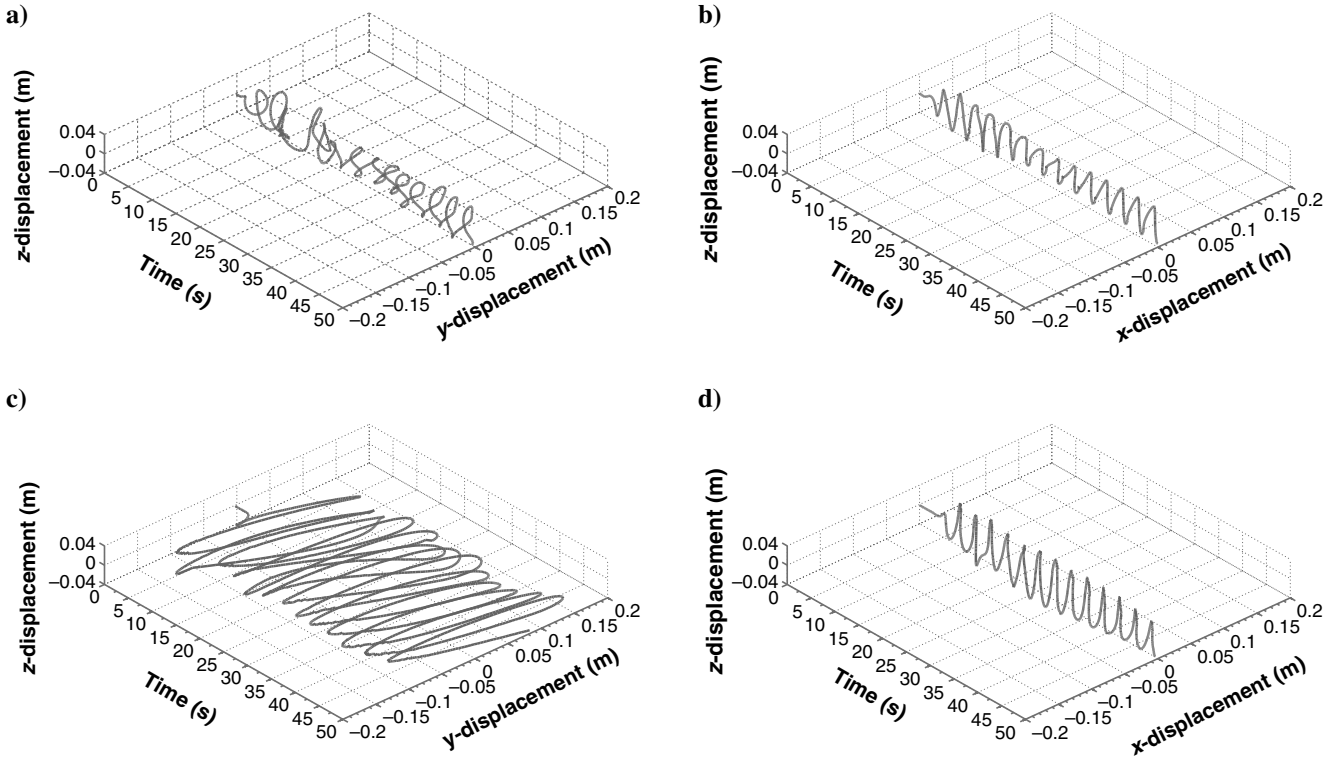

Figure 14. Trajectory of marker 5c. Panels (a) y-z, displacement for the wave in line with streamer, (b) x-z-displacement for the wave in line with streamer, (c) y-z-displacement for the wave perpendicular to the streamer, and (d) x-z-displacement for the wave perpendicular to the streamer.

Figure 15. The average rms noise level in the time domain as a function of water flow rate: 0, 0.5, 1, and 1.5 m/s. The average rms noise level for a wave parallel to the streamer and flow rate of 0.5 m/s is shown in green.

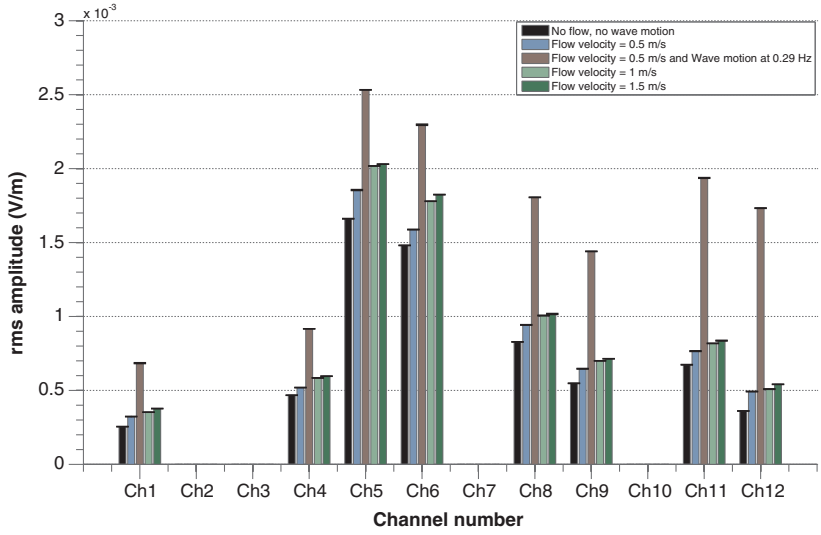

in equation 2, increases by an average of 118%, 126%, and 140% above the static noise level (E_n in equation 1) for waves propagating at angles of 0°, 45°, and 90° relative to the streamer, respectively. These increases in noise are mainly due to the motion of the streamer because of the wave motion as shown in Figures 10–13.

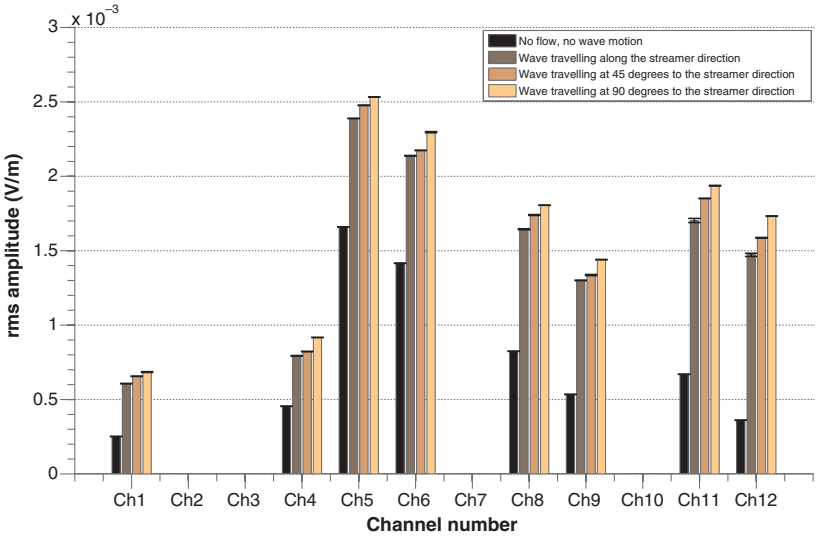

Figure 16. The average rms noise level in the time domain as a function of wave motion direction relative to the streamer.

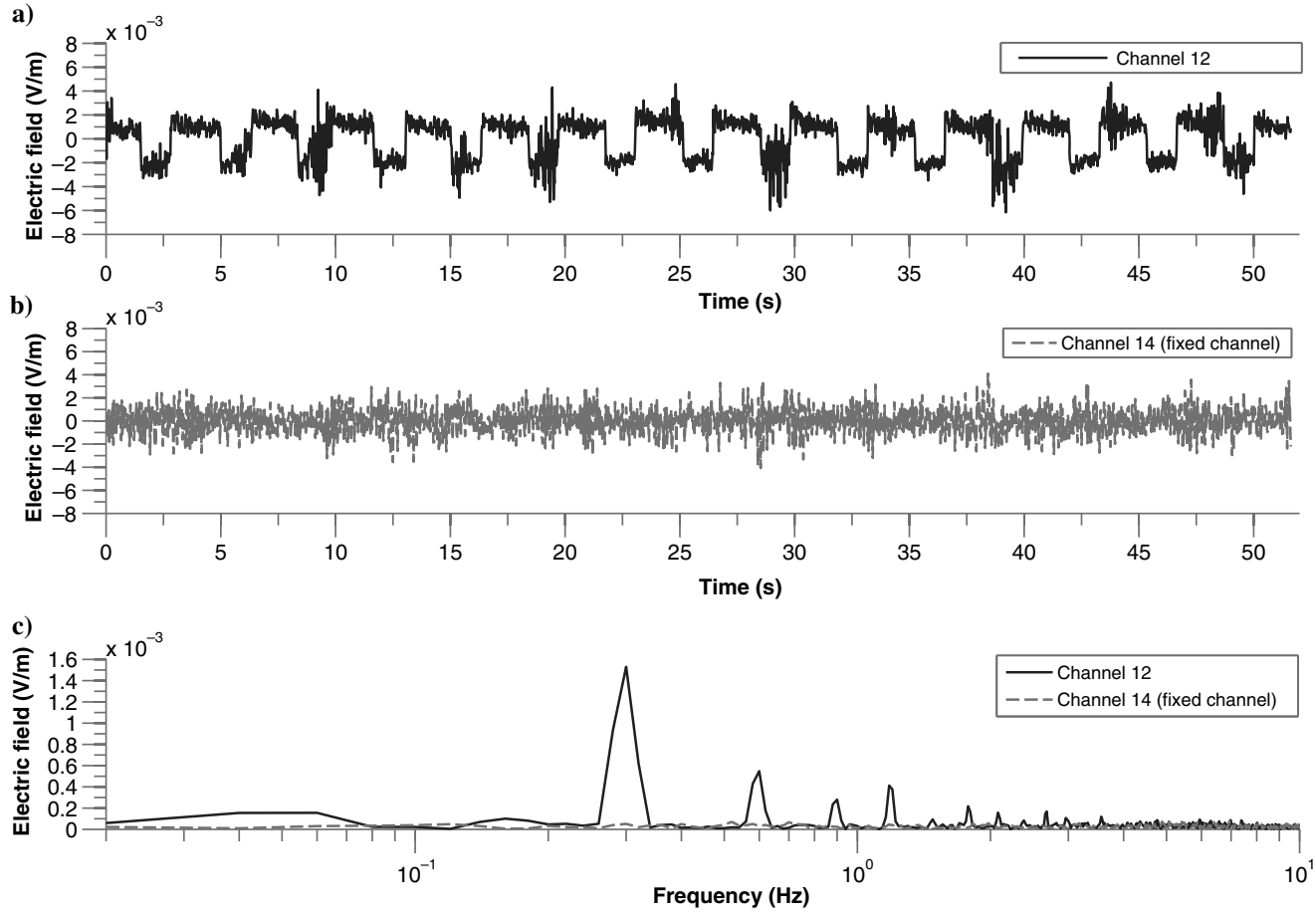

Figure 17. Data from channel 12 (inside the streamer) and channel 14 (fixed channel). Panel (a) displays electric field data recorded by channel 12, panel (b) displays electric field data recorded by channel 14, and panel (c) displays amplitude spectrum data shown in panels (a and b).

These results indicate that the increase in flow rate and wave motion at frequency of 0.29 Hz increase the noise level in the towed EM system. The increase due to wave motion is approximately twice that due to the increase in flow rate. For longer receivers, this relative difference will increase.

Isolating induction noise

We compared the electric field noise data measured on the channels inside the streamer with the electric field measured on the fixed channels (13–14) outside the streamer. These data were recorded at the same time as the data shown in Figure 11. Figure 17a and 17b shows data acquired using channels 12 (inside the streamer, 6 m apart) and 14 (fixed electrodes, 6 m apart), respectively. The effect of the wave motion can be seen on channel 12 but not on channel 14. The noise seen on channel 12 is induced by the motion of the cable in response to the wave. The amplitude spectrum in Figure 17b clearly shows large peaks at the fundamental wave frequency (0.29 Hz) and its harmonics on channel 12, but not on channel 14. There is a clear evidence that the motion of the streamer in response to waves causes noise to be induced in the streamer.

Coherence analysis

Magnitude squared coherence $C_{ab}(f)$ is a signal processing tool that provides a measure of how well two time series are correlated as a function of frequency. It varies between zero and one, where zero means completely uncorrelated and 1 means perfectly correlated:

$$C_{ab}(f) = \frac{|P_{ab}(f)|^2}{P_{aa}(f)P_{bb}(f)}, \tag{13}$$

where a and b are the input signals, $P_{ab}(f)$ is the cross power spectral density of a and b, $P_{aa}(f)$ and $P_{bb}(f)$ are the power spectral density of a and b, respectively, at each frequency component f. Coherence is used here to investigate the correlation between the measured electric field and the streamer motion.

Figure 18a and 18b shows that there is a strong correlation (≈0.91) between channels inside the streamer and wave motion. In contrast, the correlation is very low (≈0.12) between the fixed channel outside the streamer and wave motion. These results confirm that channels inside the streamer are sensitive to wave motion. Fixed electrodes with the signal cable out of the water are not sensitive to wave motion. This clearly illustrates the effect of induction noise due to the streamer moving in the earth's magnetic field.

The experiment allows us to isolate the contribution of water motion and the resulting motion of the streamer. A 16 m long streamer is different from an 8 km streamer in many ways; for example, the tension is much less. However, this has a very little effect on flow noise. The FloWave tank is a place where the mechanisms of noise generation in the streamer can be studied in a very controlled man-

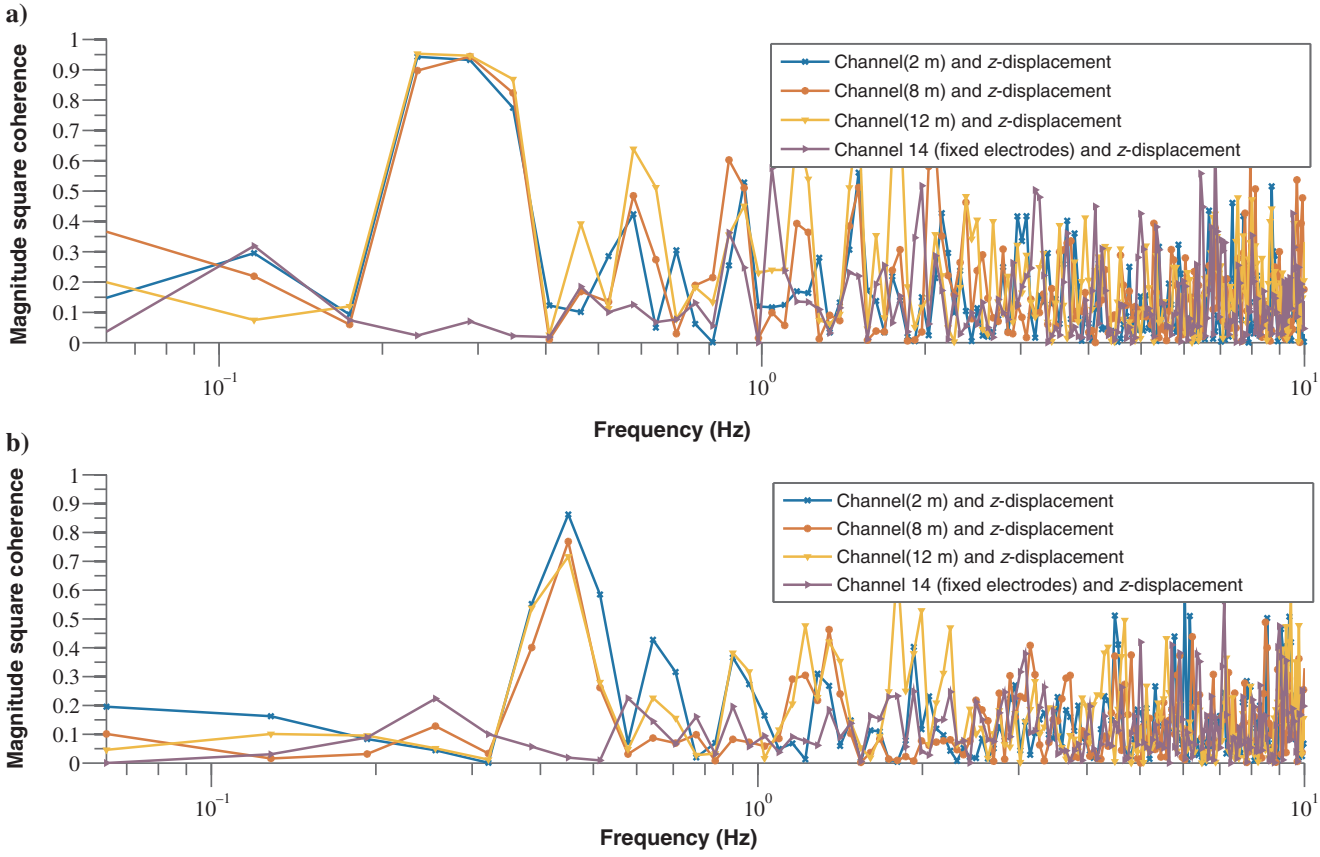

Figure 18. Magnitude squared coherence of electric field and z-displacement data. Panels (a and b) show wave frequencies 0.29 and 0.45 Hz, respectively.

ner. The results showing how the electric field is affected by streamer motion are applicable to any motion of the cable not just wave motion of course and the same mechanism of course applies to long streamers. In the absence of any method for prediction and subtraction, the noise can only be reduced by not recording it in the first place. This means limiting the lateral motion of the cable while towing, which may involve using very long streamers or towing the cable deeper. Longer receivers also enable some canceling of induction noise by averaging, but this is at the expense of spatial resolution.

CONCLUSIONS

We have looked at EM induction in a towed EM streamer. A simple analysis of a horizontal streamer in a constant uniform magnetic field shows that there is no induced noise. We have described an experiment to identify the contributions of water flow and wave motion to the induced noise. By using motion-capture cameras, we have been able to capture the motion of the streamer in real time. The streamer was found to experience its largest displacement in the horizontal direction when the wave was propagating perpendicular to the streamer.

The noise level was found to increase with increasing flow velocity. Significant flow noise is generated even for low flow rates and does not increase greatly at greater than 0.5 m/s. However, flow noise is a much smaller component than induction noise due to wave motion even for a small 16 m long streamer.

We found that the major component of the noise was due to the motion of the streamer as a result of wave motion. Telluric cables inside the streamer are sensitive to wave motion, whereas fixed electrodes with telluric cables out of the water are insensitive to wave motion. This observation provides clear evidence that the noise is due to the motion of the telluric cable in the earth's magnetic field.

To improve the overall signal-to-noise ratio of the marine-towed EM system, the motion of the streamer needs to be minimized.

ACKNOWLEDGMENTS

A. T. Djanni thank Petroleum Geo-Services for sponsoring his research. We thank the Royal Academy of Engineering for a grant to purchase the equipment for the FloWave tank experiment, and we thank the team at the Edinburgh FloWave tank for excellent cooperation during the experiment. We also thank three anonymous reviewers whose comments and suggestions have greatly improved this paper.

REFERENCES

Anderson, C., and J. Mattsson, 2010, An integrated approach to marine electromagnetic surveying using a towed streamer and source: First Break, **28**, 71–75.

Burrows, M. J., 1974, Motion-induced noise in electrode-pair extremely low frequency (ELF) receiving antennas: IEEE Transactions on Communications, **22**, 540–542, doi: 10.1109/TCOM.1974.1092213.

Cheng, D. K., 1989, Field and wave electromagnetics: Addison-Wesley.

Connell, D., and K. Key, 2013, A numerical comparison of time and frequency-domain marine electromagnetic methods for hydrocarbon exploration in shallow water: Geophysical Prospecting, **61**, 187–199, doi: 10.1111/j.1365-2478.2012.01037.x.

Constable, S., 2013, Review paper: Instrumentation for marine magnetotelluric and controlled source electromagnetic sounding: Geophysical Prospecting, **61**, 505–532, doi: 10.1111/j.1365-2478.2012.01117.x.

Constable, S., P. Kahnberg, K. Callaway, and D. Mejia, 2012, Mapping shallow geological structure with towed marine CSEM receivers: 82nd Annual International Meeting, SEG, Expanded Abstracts, doi: 10.1190/segam2012-0839.1.

Constable, S., and L. J. Srnka, 2007, An introduction to marine controlled-source electromagnetic methods for hydrocarbon exploration: Geophysics, **72**, no. 2, WA3–WA12, doi: 10.1190/1.2432483.

Elboth, T., B. A. P. Reif, and Ø. Andreassen, 2009, Flow and swell noise in marine seismic data: Geophysics, **74**, no. 2, Q17–Q25, doi: 10.1190/1.3078403.

Engelmark, F., and J. Mattsson, 2013, Estimating vertical and horizontal resistivity of the overburden and the reservoir for the Alvheim — Boa field: 83rd Annual International Meeting, SEG, Expanded Abstracts, 856–859, doi: 10.1190/segam2013-0764.1.

Engelmark, F., J. Mattsson, and J. Linfoot, 2012, Efficient marine CSEM with a towed acquisition system: Presented at the 21 EM Induction Workshop.

Filloux, J. H., 1973, Techniques and instrumentation for study of natural electromagnetic induction at sea: Physics of Earth and Planetary Interior, **7**, 323–338, doi: 10.1016/0031-9201(73)90058-7.

Gamble, T. D., W. M. Goubau, and J. Clarke, 1979, Magnetotellurics with a remote magnetic reference: Geophysics, **44**, 53–68, doi: 10.1190/1.1440923.

Krail, P. M., and H. Brysk, 1989, The shape of a marine streamer in a cross current: Geophysics, **54**, 302–308, doi: 10.1190/1.1442655.

Ronaess, M., and P. Lindqvist, 2010, Method and apparatus for reducing induction noise in measurements made with a towed electromagnetic survey system: U.S. Patent 7,671,598 B2.

Sheiman, J. L., 1990, Method for processing marine seismic data: U.S. Patent 4,974,212.

Simpson, F., and K. Bahr, 2005, Practical magnetotellurics: Cambridge University Press.

Tenghamn, S. R. L., R. J. M. Mattson, P. G. Krylstedt, M. F. Karlsson, U. P. Lindqvist, and P. A. Davidsson, 2007, Low noise, towed electromagnetic system for subsurface exploration: U.S. Patent 2007/0229083 A1.

Ziolkowski, A. M., and R. G. Carson, 2014, Method for reducing induction noise in towed marine electromagnetic survey signals: U.S. Patent 8,649,992 B2.